Thermocatalysis enables photocatalytic oxidation of methane to formic acid at room temperature beyond the selectivity limits

Di Hu, Ahmed Addad, Karima Ben Tayeb Meziane, Vitaly Ordomsky, Andrei Khodakov

Cell Reports
Physical Science

CellPress
OPEN ACCESS

Article

Thermocatalysis enables photocatalytic oxidation of methane to formic acid at room temperature beyond the selectivity limits

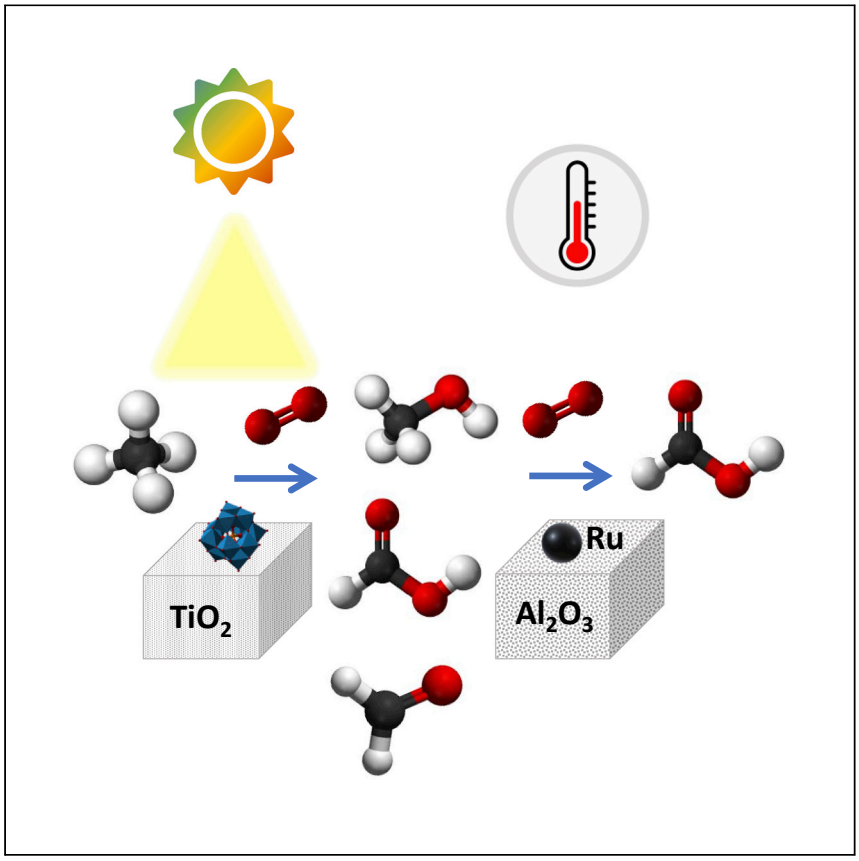

The direct oxidation of methane into fuels and chemicals remains an important challenge for modern science. Hu et al. report a strategy for highly selective one-pot synthesis of formic acid from methane by a combination of photo- and thermocatalysis at room temperature.

Di Hu, Ahmed Addad, Karima Ben Tayeb, Vitaly V. Ordomsky, Andrei Y. Khodakov

vitaly.ordomsky@univ-lille.fr (V.V.O.)
andrei.khodakov@univ-lille.fr (A.Y.K.)

Highlights

Combing photocatalysis and thermocatalysis

Room temperature single-pot reactor process

Selective synthesis of formic acid from methane

Heteropolyacid catalyst supported on titania

Hu et al., Cell Reports Physical Science 4, 101277
February 15, 2023
https://doi.org/10.1016/j.xcrp.2023.101277

Cell Reports
Physical Science

CellPress
OPEN ACCESS

Article

Thermocatalysis enables photocatalytic oxidation of methane to formic acid at room temperature beyond the selectivity limits

Di Hu,[1] Ahmed Addad,[2] Karima Ben Tayeb,[3] Vitaly V. Ordomsky,[1,*] and Andrei Y. Khodakov[1,4,*]

SUMMARY

Direct conversion of methane into fuels and chemicals remains a major challenge in modern science. Formic acid is one of the most promising platform molecules. Photocatalysis proposes an attractive route for methane partial oxidation under mild conditions. The radical mechanism of methane photocatalytic oxidation restricts the selectivity to target products. In this article, we propose a strategy to break conventional limitations of methane photocatalytic oxidation by adding a thermocatalyst and conducting the process in a one-pot reactor. In this strategy, the methane selective conversion into formic acid proceeds first over cesium salt of phosphotungstic acid on titania, which photocatalytically oxidizes methane into a mixture of C_1 oxygenates. These oxygenates are then selectively converted into formic acid over a heterogeneous alumina-supported ruthenium catalyst. All reactions occur at room temperature in the same reactor. A selectivity to formic acid of 85% and a productivity of 5 mmol $g^{-1}_{photocatalyst}$ are achieved.

INTRODUCTION

Methane, the main component of natural and shale gas, gas hydrate, and biogas is a promising feedstock for the chemical industry but, at the same time, an extremely inert molecule.[1–6] The chemical stability of methane is closely related to high C–H bond energy (439 kJ mol^{-1}) and its symmetric tetrahedral molecular geometry, which lead to low polarizability, weak acidity, and low affinity for electrons and protons.[7–9] As a result, methane is currently burned for energy production and accounts for 20%–25% of global carbon dioxide emissions into the atmosphere.[10] Moreover, methane "flaring" (methane burning at the oil production sites) consumes around 3.5% of the global amount of produced natural gas. Methane is itself a greenhouse gas (GHG) with an impact on the climate 30 times[11,12] higher than carbon dioxide.

Currently available industrial technologies of methane utilization involve indirect and direct highly energy-intensive thermochemical processes. The indirect two-step processes occur through intermediate production of syngas (mixture of hydrogen and carbon monoxide)[5,13,14] by steam reforming (Equation 1) or partial oxidation (Equation 2) at a temperature higher than 800°C:

$$CH_4 + H_2O\ (g) \rightarrow CO + 3H_2,\ \Delta H^0_{298K} = 205.9\ kJ\ mol^{-1} \quad \text{(Equation 1)}$$

$$CH_4 + 1/2\ O_2 \rightarrow CO + 2H_2,\ \Delta H^0_{298K} = -36\ kJ\ mol^{-1} \quad \text{(Equation 2)}$$

[1]University Lille, CNRS, Centrale Lille, University Artois, UMR 8181 – UCCS – Unité de Catalyse et Chimie du Solide, 59000 Lille, France

[2]University Lille, CNRS, INRAE, Centrale Lille, UMR 8207 - UMET - Unité Matériaux et Transformations, 59000 Lille, France

[3]University Lille, CNRS, UMR 8516 – LASIRE – Laboratoire de Spectroscopie pour les Interactions, la Réactivité et l'Environnement, 59000 Lille, France

[4]Lead contact

*Correspondence: vitaly.ordomsky@univ-lille.fr (V.V.O.), andrei.khodakov@univ-lille.fr (A.Y.K.)

https://doi.org/10.1016/j.xcrp.2023.101277

In the second step, the produced syngas is converted[15–18] to chemicals and fuels. The only available industrial technologies for direct thermochemical methane utilization are the Andrussow process and the non-oxidative BMA (or Degussa) process, in which methane reacts with ammonia at extremely high temperatures (>1,600°C) and produces hydrogen cyanide.[19]

Photocatalysis is a promising strategy for converting solar light into chemical energy, and it may enable activation of C–H bonds in methane under mild conditions.[20–23] Recently, photocatalysis has demonstrated great potential for methane conversion to fuels and chemicals at room temperature.[13,24–27]

Several photocatalytic systems and oxidants have been explored for methane oxidation to oxygenates (Table S1; supplemental information). Photocatalytic aerobic oxidation of methane to methanol over Au/ZnO[28,29] and Au-CoO_x/TiO_2[30] has been recently reported. The boosted performance of these catalysts was attributed to mild oxidative hydroperoxyl radicals (•OOH) produced over the co-catalysts. Methane oxidation to methanol has been observed over FeO_x/TiO_2[31] in the presence of H_2O_2 at ambient conditions, resulting from lower overpotential of H_2O_2 reduction to hydroxyl radicals (•OH) over iron species. Toxic and unstable chlorine dioxide radicals were also used[32] for the non-catalytic synthesis of formic acid from methane. Besides, photocatalytic aerobic oxidation of methane to formaldehyde and formic acid was reported over Au_x/c-WO_3[33] and HSiMo/TiO_2.[34] The process, however, required either high pressure or an elevated temperature. Because of the radical mechanism of methane photocatalytic oxidation, multiple liquid oxygenates (methyl hydroperoxide, methanol, formaldehyde, formic acid, etc.) are usually simultaneously produced and can be hardly separated. Most of the current photocatalytic methane oxidation routes suffer from insufficient selectivity and low productivity or require highly reactive, unstable, and toxic oxidants (H_2O_2, ClO_2, etc.).

Formic acid is one of the most promising feedstocks[35,36] for hydrogen storage, fuel cells, grass silage, leather tanning, textile dyeing, finishing, food additives, natural rubber, drilling fluids, and various chemical processes. Currently, industrial production of formic acid proceeds via a multistep process that involves methanol carbonylation with subsequent hydrolysis of methyl formate.[33,35] Direct selective transformation of methane to formic acid occurring at room temperature using renewable energy sources such as solar light and without any toxic oxidants could be, therefore, extremely attractive and valuable.

Hereby, we propose a strategy for synthesizing formic acid from methane with a selectivity that exceeds the usual limitations of photocatalysis. The process takes place in water at ambient temperature and employs air as an oxidant (Figure 1). The process involves two catalytic systems. Methane photocatalytic oxidation over cesium salt of phosphotungstic acid ($H_3O_{40}PW_{12}$, HPW) supported on titania is used for the synthesis of a mixture of C_1 oxygenates (methyl hydroperoxide, methanol, formaldehyde, and formic acid). Insoluble cesium salt was used for heterogenization of heteropolyacid, which is soluble in aqueous solutions. A heterogeneous ruthenium catalyst supported by alumina enables thermocatalytic oxidation of C_1 oxygenates to formic acid. Highly selective methane oxidation to formic acid is achieved under ambient temperature. The formic acid productivity has reached 5 $mmol_{formic\ acid}\ g^{-1}{}_{photocatalyst}$ with a selectivity of 85%. A concentrated formic acid solution of 1.1 mmol L^{-1} is produced in this process.

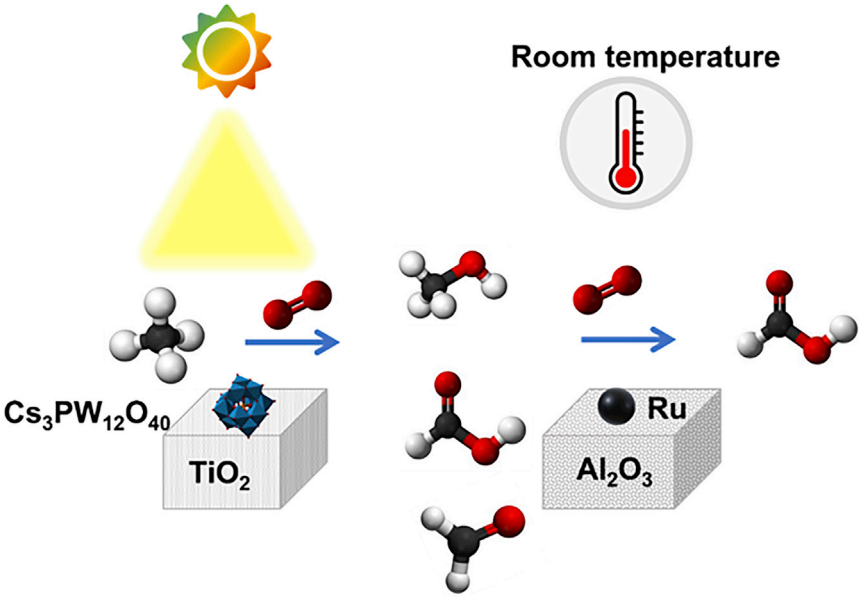

Figure 1. Photothermocatalytic process
Selective synthesis of formic acid from methane at room temperature.

RESULTS AND DISCUSSION

Photocatalytic methane oxidation with O_2 in water to a mixture of C_1 oxygenates

First, the photocatalytic methane oxidation was investigated at ambient temperature in the presence of the following photocatalysts: HPW, cesium salt of HPW (CsPW), and TiO_2 (Figure 2A). No methane conversion is observed in the reactor with any of these catalysts in the absence of light, indicating that methane oxidation is driven by photocatalysis. Under irradiation, without a catalyst, only a small amount of formaldehyde has been detected (Figure 2A). Some minor formaldehyde formation from CH_4 under UV irradiation has been previously reported in the literature.[37,38] Also, very low methane conversion was observed over the catalysts in the presence of light but without oxygen. The methane oxidation without a catalyst or in the absence of oxygen can be due to the hydroxyl radicals generated[37,38] by UV light in water.

Exposure of the reactor with HPW and CsPW to methane and oxygen under irradiation also results in formaldehyde generation (Figure 2A). The amount of formaldehyde produced over HPW and CsPW was, however, also very small, similar to that detected in the reactor under irradiation without any catalyst. This suggests that HPW or CsPW are not active in methane photocatalytic oxidation. Much higher amounts of formaldehyde and CO_2 were produced from methane under irradiation in the reactor filled with TiO_2. Note that methane oxidation over TiO_2 is accompanied by a major production of CO_2. The observed photocatalytic activity of TiO_2 in methane oxidation to formaldehyde and CO_2 is consistent with previous studies.[28,39]

Very different selectivity patterns were observed, however, in the methane photocatalytic conversion over the CsPW-TiO_2 catalyst. A mixture of C_1 oxygenates in larger amounts was detected on CsPW-TiO_2; formic acid is one of the main oxidation products (Figure 2A). Important, the selectivity to undesirable CO_2 was significantly reduced over CsPW-TiO_2 compared with titania.

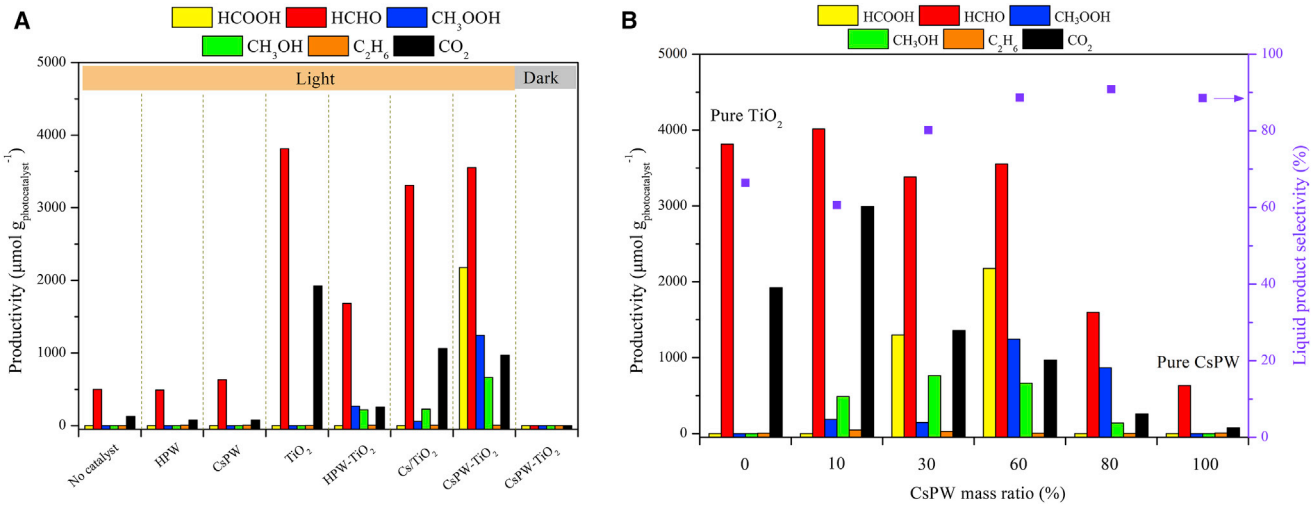

Figure 2. Methane photocatalytic oxidation with air in water

Methane photocatalytic oxidation with air in water over various composites (A) and over CsPW-TiO_2 with different CsPW mass ratios (B). Reaction conditions: 10 mg catalyst, 100 mL water, 0.6 MPa CH_4, 0.1 MPa air, 2 h reaction time, 20°C ± 2°C reaction temperature, light source: 400 W Hg-Xe lamp, full irradiation.

Note that no formic acid was detected in the methane photocatalytic oxidation over HPW-TiO_2 and Cs/TiO_2 (Figure 2A). The selectivity patterns of HPW-TiO_2 are similar to that of TiO_2. It is well known that HPW is readily soluble in polar solvents.[40] The observed inferior catalytic performance of HPW-TiO_2 with selectivities similar to those of TiO_2 is possibly due to leaching HPW from the surface of TiO_2. Consequently, methane oxidation to CO_2 and formaldehyde occurs on TiO_2 surface sites in HPW-TiO_2 and Cs/TiO_2.

Much higher oxygenate yields compared with HPW-TiO_2, accompanied by the major production of formic acid, are observed on all the insoluble HPW salts (CsPW, AgPW, NH_4PW) mixed with TiO_2 (Figure S1). Note that over the AgPW-TiO_2 and NH_4PW-TiO_2 samples, the formic acid productivity was somewhat lower compared with CsPW-TiO_2. The Ag^+ cations in AgPW may undergo a reduction to metallic silver, which is detected by X-ray diffraction (XRD) in the spent AgPW-TiO_2 catalyst (Figure S2), while the NH_4^+ cations can decompose under irradiation. Both processes may lead to the formation of soluble HPW, its leaching from TiO_2,[41,42] and loss of catalytic activity. Insoluble and stable CsPW demonstrates superior stability in the aqueous solution under irradiation. The XRD shows that the spent CsPW-TiO_2 catalyst is intact compared with the fresh one (Figure S3). Stable catalytic performance was observed over CsPW-TiO_2 in 4 catalytic cycles (Figure S4). These results indicate the indispensable role of Cs^+ ions in stabilizing HPW on the surface of TiO_2 during efficient photocatalytic methane oxidation. Several types of heteropolyacids such as phosphotungstic acid, phosphomolybdic acid, silicomolybdic acid, and silicotungstic acid were also used for the preparation of cesium-heteropolyacid titania nanocomposites (Figure S5). The overall methane conversion was much lower over the catalysts prepared by mixing Cs of phosphomolybdic and silicomolybdic acids and TiO_2 compared with CsPW-TiO_2.

The formic acid productivity as a function of CsPW content in the CsPW-TiO_2 catalysts displays a volcano-type curve (Figure 2B). Lower formic acid productivity at low content of CsPW can be due to the contribution of TiO_2 to methane oxidation

to formaldehyde and CO_2, while insufficient light harvesting at low content of TiO_2 can explain low formic acid production at a higher amount of CsPW in CsPW-TiO_2. Very low methane conversion was observed under anaerobic conditions, with formaldehyde being the major product. The oxygenate yield over CsPW-TiO_2 is boosted in air (Figure S6). At higher methane relative content, lower formic acid productivity was observed, which can be due to the deficiency of oxygen in the reactor required for methane oxidation (Figure S7).

The methane photocatalytic oxidation over CsPW-TiO_2 was studied as a function of reaction time (Figure S8). As expected, methane conversion increases with irradiation time. At a shorter reaction time, the methane conversion mostly leads to formaldehyde and methyl hydroperoxide. Formic acid has been only observed at a longer reaction time. This suggests that formic acid is principally produced by re-oxidation of formaldehyde and possibly methyl hydroperoxide. The selectivity to CO_2 also increases with reaction time, most probably due to re-oxidation of C_1 oxygenates. To prove possible re-oxidation of HCHO to HCOOH and CO_2 under irradiation, CsPW-TiO_2 was dispersed in HCHO solution (500 μmol L^{-1}) (Figure S9). An HCOOH yield of 11.76 μmol was achieved from the direct HCHO oxidation in 2 h. The suggestion about re-oxidation of C_1 oxygenates generated by methane photocatalytic oxidation is also confirmed by the experiments with larger amounts of water added to the reactor. The selectivity to formic acid increases with the increase in water amount in the reactor because of the lower probability of its re-oxidation to CO_2 in the diluted solution (Figure S10).

The enhanced CsPW-TiO_2 photocatalytic performance in the methane oxidation to C_1 oxygenates and formic acid can be attributed to the formation of a p-n semiconductor heterojunction between TiO_2 and CsPW reported in the previous studies.[20,41,43,44] The valence band energy was measured by X-ray photoelectron spectroscopy (XPS). The top of the valence band was located for CsPW and TiO_2 at approximately 2.4 and 3 eV, respectively (Figure S11). Then, the position of the bottom of the conduction band for both compounds was calculated from the band-gap energy measured for the optical spectra and Tauc's plots (Figures S12 and S13). The bottoms of the conduction band for CsPW and TiO_2 were higher than the tops of the valence band by 3.28 and 3.34 eV, respectively. The band structure for TiO_2 is consistent with a previous report.[45]

The scanning transmission electron microscopy (STEM) high-angle annular dark-field (HAADF) and STEM energy-dispersive X-ray (EDX) maps (Figure 3) show close contact but a distinct separation of TiO_2 and CsPW semiconductor phases, confirming the presence of a heterojunction. Interestingly, after exposure to methane without air in the presence of light, the CsPW-TiO_2 sample becomes blue, indicating a partial reduction of W species. The catalyst gets white again after exposure to air (Figure S14). The color remains unchanged during the methane photocatalytic oxidation in air.

Methane oxidation experiments were carried out under both visible and UV light (Figure S15). No methane conversion was observed under visible light, while the methane oxidation at 360 nm UV light produced a mixture of HCHO, CH_3OOH, and CH_3OH, indicating that UV light was necessary to photoexcite CsPW-TiO_2 for methane activation. The apparent quantum yield (AQY) was 4.5% at 360 nm for CsPW-TiO_2.

The reactive oxygen species scavenging experiments were conducted during photocatalytic methane oxidation using salicylic acid and sodium sulfite (Na_2SO_3) as

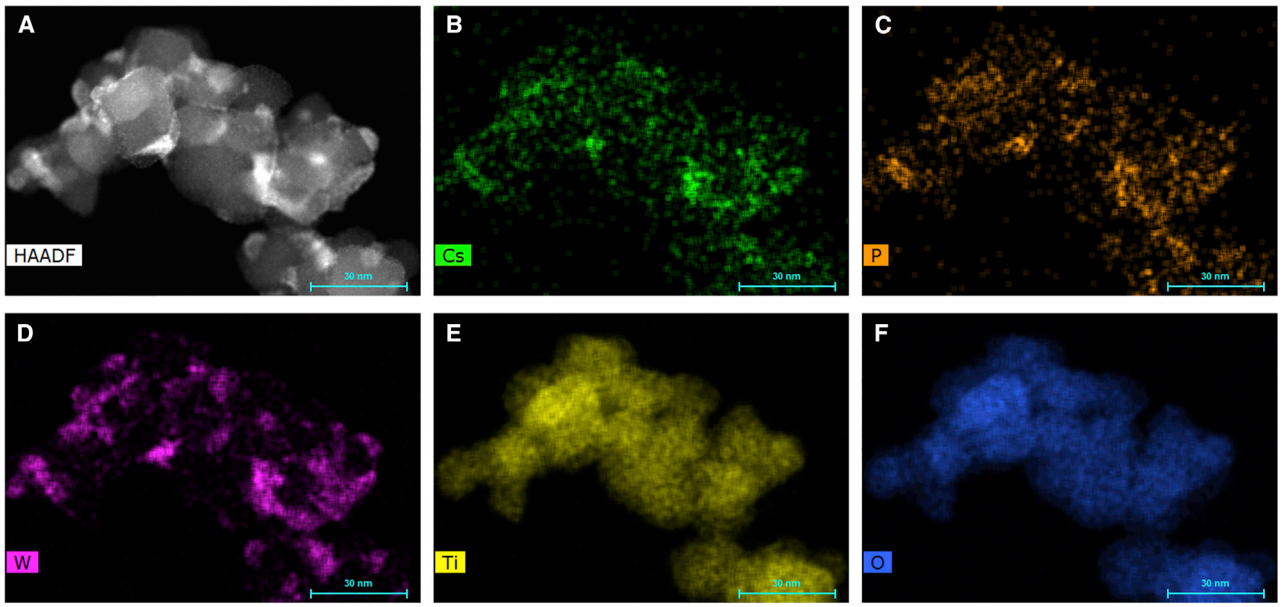

Figure 3. STEM and STEM-EDX mapping images

STEM and STEM-EDX mapping images of fresh CsPW-TiO_2 sample.

STEM-HAADF (A) and corresponding EDX mapping images of the elements: Cs (B), P (C), W (D), Ti (E), and O (F).

·OH radicals and holes (h^+) sacrificial agents, respectively.[46–48] The addition of both salicylic acid and sodium sulfite significantly suppressed methane conversion (Figure S16), suggesting that both the •OH radicals and holes (h^+) are the main reactive species for methane conversion.

To further investigate the mechanism of methane photooxidation, we measured *in situ* electron paramagnetic resonance (EPR) with 5,5-dimethyl-1-pyrroline N-oxide (DMPO) used as spin trap. Before the introduction of CH_4, only the 1:2:2:1 quartet signal ascribed to the DMPO-OH adduct was observed on illuminated CsPW-TiO_2 (Figure 4A), revealing the presence of •OH. Under air and CH_4, we observed $\bullet CH_3$ radicals with a CsPW-TiO_2 catalyst, which are not observed with pure TiO_2 (Figure 4B). In addition, CsPW-TiO_2 shows a higher DMPO-OH signal intensity than bare TiO_2 (Figure 4A), which can be due to better charge separation via the p-n heterojunction. This phenomenon is consistent with the photoluminescence (PL) spectra (Figure S17) and methane photooxidation performance.

It is well known that the adsorbed O_2 on the surface of catalysts is a strong electron scavenger[49] that can produce •OH radicals[50] and contribute to charge separation and methane oxidation. To investigate the activation of O_2 over catalysts and understand the underlying mechanism in photocatalytic methane oxidation, *in situ* EPR experiments were carried out in air or in vacuum. The EPR spectra were recorded under dark and light irradiation conditions at 120 K (Figure S18). The signal with g_1 = 2,024, g_2 = 2,013, and g_3 = 2,006 was attributed[51] to the [Ti^{4+}-O^{2-}-Ti^{4+}-$OH^{\bullet -}$] radicals. Note that under irradiation in air, the signal intensities of the O^- reactive oxygen species (ROS) over TiO_2 are stronger than that over CsPW-TiO_2, while the DMPO-OH intensity over TiO_2 is lower than CsPW-TiO_2 (Figure 4). This suggests that the abundant ROS on surface might be the main cause for the overoxidation to CO_2 over TiO_2 instead of •OH radicals over CsPW-TiO_2.

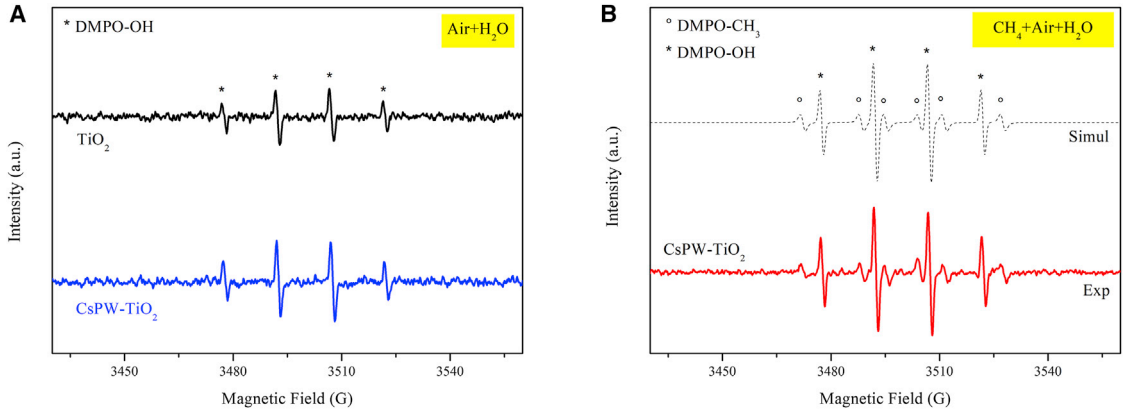

Figure 4. EPR spectra

EPR spectra of CsPW-TiO_2 and TiO_2 under irradiation in air and H_2O (A) and in methane, air, and H_2O (B). DMPO was added to the reaction mixture as the radical trapping agent.

On the basis of the above results, we propose a potential mechanism for photocatalytic methane oxidation over CsPW-TiO_2 (Figure 5). The energies of valence and conduction bands in CsPW and TiO_2 were calculated from XPS and UV-visible diffuse reflectance spectra (Figures S11–S13). Under irradiation, the charge separation is enhanced thanks to the p-n heterojunction, and the photogenerated electrons can efficiently transfer to TiO_2, while the holes migrate to CsPW. As a result, more electrons and holes are available for methane oxidation, which simultaneously oxidize H_2O via photoholes and reduce O_2 via photoelectrons for the formation of •OH radicals (Figure 4), a key factor for CH_4 activation.[48,50] The reduction of O_2 may involve a partial reduction of W species, which can also play a role as a co-catalyst. The formed •OH radicals and holes activate methane to $•CH_3$, which reacts with O_2 to form[52] CH_3OOH. The CH_3OH can derive from either the CH_3OOH precursor through a photoreduction process or the coupling of $•CH_3$ and •OH.[28] Finally, HCHO and HCOOH can be produced from the photooxidation of CH_3OH by photogenerated holes or •OH.[53]

Despite the observed high methane conversion rate, the photocatalytic oxidation of methane, which occurs at room temperature, suffers from insufficient selectivity. Indeed, methane photocatalytic oxidation over CsPW-TiO_2 results in a mixture of C_1 oxygenates (Figure 2). The separation of individual liquid oxygenates from the reaction solution can be a difficult task and prohibitively expensive. It is much more attractive and promising to achieve a selective one-pot synthesis of concentrated formic acid in the liquid phase directly from methane. That was the reason why we attempted to further selectively convert the mixture of C_1 oxygenates produced by photocatalysis into formic acid.

Thermocatalytic oxidation of methanol and formaldehyde over a commercial Ru/Al_2O_3 heterogeneous catalyst at room temperature

A series of heterogeneous supported transition metal catalysts have been investigated in a batch reactor in the formaldehyde and methanol thermocatalytic oxidation (without irradiation) to formic acid at ambient temperature in the presence of air. No conversion of methanol and formaldehyde was observed in the absence of catalyst.

No noticeable formaldehyde oxidation was observed over either CuO, Fe_2O_3, or CuZnAl (Table S2, entries 1–3). Interestingly, only supported noble metals (Pt, Pd,

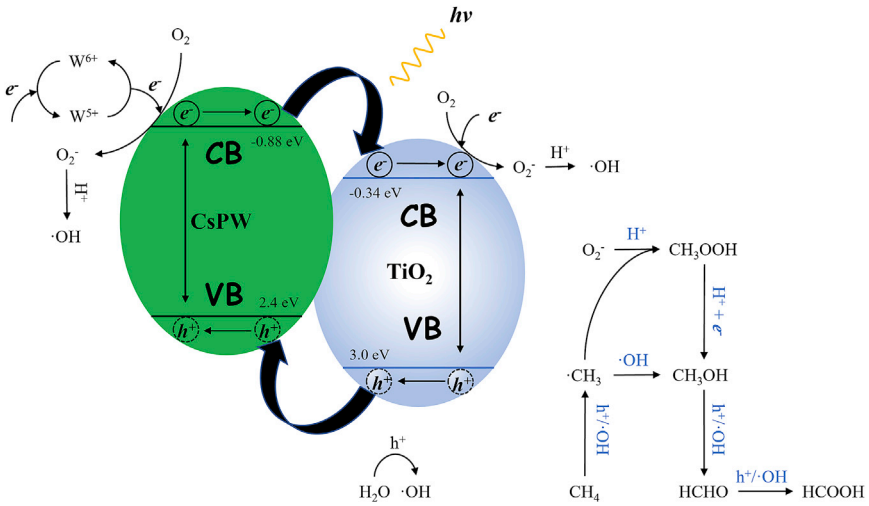

Figure 5. Reaction mechanism of photocatalytic methane oxidation

Sketch of the proposed reaction mechanism of photocatalytic methane oxidation to CH_3OOH, CH_3OH, HCHO, and HCOOH over CsPW-TiO_2. CB, conduction band; VB, valence band.

and Ru) were effective in the formaldehyde oxidation (Table S2, entries 4–7). Formaldehyde oxidation over the Pt/C and Pd/Al_2O_3 catalysts yielded only CO_2, as no liquid products were even observed. The loading of Ru can increase the concentration of oxygen vacancies on the Ru/Al_2O_3 catalyst and is therefore beneficial to the O_2 activation.[54] The formate ($HCOO^-$) species are known as the key intermediate in HCHO oxidation to HCOOH.[54,55] The conversion of adsorbed formaldehyde to the surface formate involves oxygen species on the catalyst surface. In the presence of water, the recombination of the formate with surface protons leads to the release of HCOOH into the liquid phase. The protons form on the surface via the dissociative adsorption of H_2O and HCHO.[55,56] At the same time, CO_2 forms via parallel pathways, resulting both from the HCHO oxidation and from the oxidation of adsorbed formic acid.

To study the oxidation efficiency of C_1 oxygenates mixture to formic acid, different amounts of Ru/Al_2O_3 catalyst were dispersed into 5 g (500 μmol L^{-1}) HCHO solution. Figure S19 shows that the rate of HCHO oxidation into HCOOH increases with an increase in the amount of Ru/Al_2O_3 catalyst. The complete oxidation of HCHO with 0.01 g Ru/Al_2O_3 takes a rather long time (about 48 h). We chose 0.1 g Ru/Al_2O_3 for efficient oxygenate oxidation in the cascade process. Important, Ru/Al_2O_3 showed selective thermocatalytic oxidation of formaldehyde to formic acid with a selectivity of 71%. Interestingly, even with increasing the reaction time from 2 to 12 h (Table S2, entries 6 and 7), no further oxidation of formic acid to CO_2 has been detected.

In addition to formaldehyde, the supported Ru/Al_2O_3 catalyst was evaluated in the methanol thermocatalytic oxidation at room temperature in the presence of air. The catalytic results are presented in Table S3. In the presence of Ru/Al_2O_3, methanol is oxidized with a selectivity of 64% to formic acid. The catalytic results suggest, therefore, that Ru/Al_2O_3 can be an efficient catalyst for the selective oxidation of a mixture of C_1 oxygenates produced by photocatalytic oxidation of methane to formic acid at ambient temperature. The commercial 5 wt % Ru/Al_2O_3 catalyst was characterized using a combination of techniques: XRD, imaging techniques, XPS, and temperature-programmed reduction (TPR). The details of characterization of CsPW-TiO_2

Table 1. Methane oxidation over the CsPW-TiO_2+Ru/Al_2O_3 catalysts prepared by mechanical mixing and in the combined process

		Catalyst weight composition, g		Productivity (μmol $g_{photocatalyst}^{-1}$ h^{-1})				
Entry	Catalyst	CsPW-TiO_2	Ru/Al_2O_3	CH_3OH	CH_3OOH	HCHO	HCOOH	CO_2
1[a]	CsPW-TiO_2	0.01	0	332.21	621.94	1,777.01	1,088.12	484.38
2[a]	CsPW-TiO_2+ Ru/Al_2O_3	0.01	0.1	0	0	0	0	trace
3[b]	CsPW-TiO_2+ Ru/Al_2O_3	0.01	0.01	195.75	0	300.00	0	151.80
4	combined process: separated CsPW-TiO_2 and Ru/Al_2O_3	0.01	1	0	0	0	2,528.13	446.79

Reaction conditions: 0.6 MPa CH_4, 0.1 MPa air, 100 mL water, 20°C ± 2°C reaction temperature, 400 W Xe lamp, full irradiation.
[a]2 h reaction time.
[b]5 h reaction time.

and Ru/Al_2O_3 are given in the supplemental information (supplemental experimental procedures; Figures S11–S13 and S20–S23).

Photothermocatalytic process for selective synthesis of formic acid from methane

After elaboration of photocatalytic methane oxidation to C_1 oxygenates and thermocatalytic oxidation of C_1 oxygenates to formic acid, we tried to combine these two reactions into a single process by mechanically mixing the CsPW-TiO_2 photocatalyst with the Ru/Al_2O_3 heterogeneous catalyst (Table 1). No liquid product, only traces of CO_2, was observed over the mixed composites containing 0.1 g Ru/Al_2O_3 and 0.01 g CsPW-TiO_2 (Table 1, entry 2). Small amounts of methanol and formaldehyde were eventually detected by reducing the Ru/Al_2O_3 amount in the mixed composite and extending the irradiation time (Table 1, entry 3). However, an extremely lower methane conversion over the mechanically mixed catalysts, compared with the photocatalytic performance of CsPW-TiO_2 (Table 1, entry 1; Figure 6B), indicates that the mechanical mixing completely suppresses the photocatalytic process, most probably due to covering the photocatalyst by its alumina-supported counterpart, making it inaccessible to irradiation. The UV-visible spectra (Figure S12) show an almost complete disappearance of absorption related to the band-gap transition in the TiO_2 and CsPW semiconductors after mixing with Ru/Al_2O_3.

Then, the CsPW-TiO_2 and Ru/Al_2O_3 were loaded in the same reactor but separately from each other. The reactor configuration is shown in Figures 6C and S24. The photocatalyst is located at the top of the reactor and exposed to irradiation. The ruthenium catalyst is placed under a sand filter at the bottom of the reactor. The productivities of oxygenates attained in the photocatalytic process with the CsPW-TiO_2 catalysts and the photothermocatalytic process with CsPW-TiO_2 and Ru/Al_2O_3 are shown in Table 1, entries 1 and 4, and Figure 6. Different from the photocatalytic reaction, which produced a multitude of C_1 oxygenates (Figure 6A), methane conversion in the newly designed process selectively yields formic acid (Figure 6C). After the optimization of the reaction conditions, the productivity of HCOOH reached 5,000 μmol $g_{photocatalyst}^{-1}$ after 2 h irradiation with a total selectivity of ~85%. CO_2 was the only gaseous compound, which was produced during methane oxidation.

The isotopic labeling experiments using $^{13}CH_4$ were conducted to confirm the carbon source of C_1 oxygenates. The four ^{13}C nuclear magnetic resonance (NMR) signals at 168, 82, 65, and 48 ppm (Figure 7A) were attributed to $H^{13}COOH$, $H^{13}CHO$, $^{13}CH_3OOH$, and $^{13}CH_3OH$, respectively. In addition, the existence of $H^{13}COOH$ alone after oxygenate oxidation over Ru/Al_2O_3 suggests that $^{13}CH_4$-derived

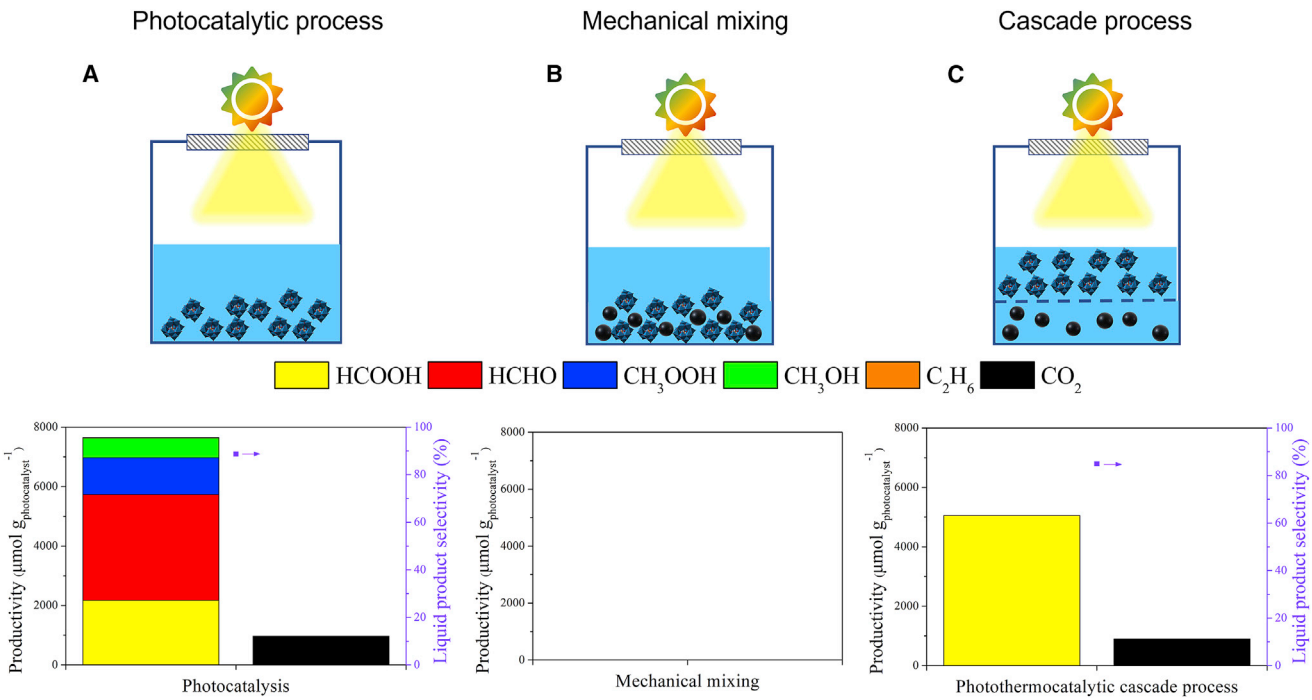

Figure 6. Methane oxidation processes

Methane oxidation in photocatalytic (A), mechanical mixing (B), and photothermocatalytic processes (C). Photocatalytic process: 10 mg CsPW-TiO_2, 100 mL water, 0.6 MPa CH_4, 0.1 MPa air, 2 h irradiation time, 20°C ± 2°C reaction temperature, light source: 400 W Xe lamp, full irradiation. Mechanical mixing: 10 mg CsPW-TiO_2, 100 mg 5% Ru/Al_2O_3, 100 mL water, 0.6 MPa CH_4, 0.1 MPa air, 2 h irradiation time, 20°C ± 2°C reaction temperature, light source: 400 W Hg-Xe lamp, full irradiation. Photothermocatalytic process: 10 mg CsPW-TiO_2, 1 g 5% Ru/Al_2O_3, 100 mL water, 0.6 MPa CH_4, 0.1 Mpa air, 2 h irradiation time followed by 0.5 h thermal catalysis (without irradiation), 20°C ± 2°C reaction temperature, light source: 400 W Hg-Xe lamp, full irradiation.

oxygenates were selectively oxidized into formic acid (Figure 7B). These results confirm that all the oxygenates indeed originate from methane.

Numerous applications require concentrated solutions of formic acid. Separation of formic acid from water can be prohibitively expensive if the concentration of the target product in the post-reaction mixture is low. To reach a higher concentration of the formic acid in the liquid phase, we reduced the amount of water (30 mL). With some decrease in the selectivity, a concentrated HCOOH solution of 1.1 mmol L^{-1} was obtained (Figure S25). This opens the way to the direct synthesis of concentrated formic acid from methane using a combined photothermocatalytic process.

In this work, we propose a one-pot photothermocatalytic process for the selective synthesis of formic acid from methane with air as an oxidant at ambient temperature. A yield of formic acid over 5,000 μmol $g_{photocatalyst}^{-1}$ and a selectivity of 85% were achieved. CO_2 is the only gaseous compound in methane oxidation. Optimization of reaction conditions allows synthesis of HCOOH solution with a concentration of 1.1 mmol L^{-1}.

The process involves a photocatalyst prepared from Cs of phosphotungstic acid mixed with titania and a heterogeneous alumina-supported ruthenium catalyst. Methane photocatalytic oxidation results in a mixture of C_1 oxygenates, which then are selectively oxidized to formic acid. Our findings offer valuable guidance for the direct and highly selective methane oxidation to HCOOH in water using O_2 as an oxidant.

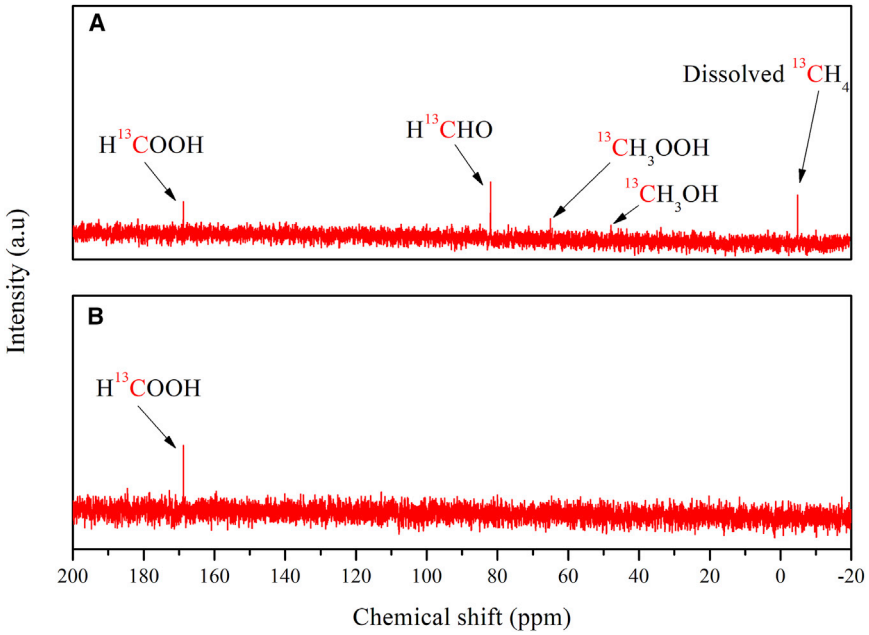

Figure 7. ^{13}C NMR spectra

^{13}C NMR spectra of the products obtained from photocatalytic methane oxidation over CsPW-TiO_2 using $^{13}CH_4$ (A) and subsequent oxygenates oxidation over Ru/Al_2O_3 (B).

This strategy can be particularly suitable for selective conversion of extremely inert molecules such as methane, light alkanes, or CO_2 under mild conditions to value-added molecules.

EXPERIMENTAL PROCEDURES

Resource availability

Lead contact

Further information and requests for resources should be directed to and will be fulfilled by the lead contact, Dr Andrei Y. Khodakov (andrei.khodakov@univ-lille.fr).

Materials availability

This study did not generate new unique reagents.

Data and code availability

The authors declare that the data supporting the findings of this study are available within the paper and supplemental information. All other data are available from the lead contact upon reasonable request.

Materials

Titanium (IV) oxide (P25, 99.5%, primary 21 nm); phosphotungstic acid hydrate ($H_3O_{40}PW_{12}\cdot xH_2O$, HPW); phosphomolybic acid hydrate ($H_3(P(Mo_3O_{10})_4)\cdot xH_2O$, HPMo); tungstosilicic acid hydrate ($H_4(Si(W_3O_{10})_4)\cdot xH_2O$, HSiW); silicomolybdic acid solution ($H_4(Si(Mo_3O_{10})_4)\cdot xH_2O$, HSiMo); HCHO solution (1,000 μg/mL); silver nitrate ($AgNO_3$, ≥99%); cesium nitrate ($CsNO_3$, ≥99%); and ammonium bicarbonate (NH_4HCO_3, ≥99%) were purchased from Sigma-Aldrich. Air and methane were supplied by Air Liquid and were used in the catalytic reactions. All chemicals were used without treatment.

Catalyst preparation

Different phosphotungstic salts (AgPW, CsPW, and NH_4PW) were prepared by mixing HPW hydrate aqueous solution with the stoichiometric amount of $AgNO_3$, $CsNO_3$, and NH_4HCO_3 aqueous solution, respectively. The Cs of different heteropolyacids (CsPW, CsPMo, CsSiW, and CsSiMo) were prepared by mixing $CsNO_3$ aqueous solution with the stoichiometric amount of heteropolyacids aqueous solution (HPW, HPMo, HSiW, and HSiMo), respectively. All the precipitated salts were then washed by deionized water three times and filtered out.

Preparation of CsPW-TiO_2

0.1 g CsPW was mechanically mixed with a necessary amount of TiO_2 to provide a specific CsPW mass ratio (10%, 30%, 60%, and 80%); preparation of the other heteropolyacid salts (AgPW, NH_4PW, CsPMo, CsSiW, and CsSiMo)-TiO_2: 0.1 g heteropolyacid salts was mechanically mixed with a necessary amount of TiO_2 to provide a 60% heteropolyacid salt mass ratio. Unless otherwise specified in this work, the mass ratio of heteropolyacid salt is 60% in all the heteropolyacid salt-TiO_2 samples.

Preparation of HPW-TiO_2

0.5 g TiO_2 was mechanically mixed with a necessary amount of HPW hydrate to provide the corresponding HPW amount as in CsPW-TiO_2.

Preparation of Cs/TiO_2

Cs/TiO_2 was prepared by incipient wetness impregnation of TiO_2 with aqueous solutions of cesium nitrate ($CeNO_3$) to provide the same amount of cesium as in CsPW-TiO_2. All the pre-synthesized samples were dried at 353 K overnight and calcined (except for NH_4PW and NH_4PW-TiO_2) at 573 K in air for 3 h with a 2°C min^{-1} temperature ramp. The commercial Ru/Al_2O_3 catalyst (5 wt % Ru) was purchased from Merck.

In the mechanically mixing experiment, 10 mg CsPW-TiO_2 was mechanically mixed with 100 mg Ru/Al_2O_3 by grinding, after which the composite mixture was directly dispersed into 100 mL water for reaction.

Photocatalytic tests

A commercial 230 mL batch photoreactor equipped with a quart window on the top was used for photocatalytic methane oxidation reaction tests (Figure S24 and S26). The light source was provided by a 400 W Hg-Xe lamp from Newport (66485-500HX-R1) with full irradiation (from ~200 to 1,100 nm). The light intensity was 0.348 W cm^{-2}.

Typically, a 10 mg sample was dispersed in 100 mL deionized water in a quartz cup, after which the quartz cup was placed into reactor, pressurized with 0.1 MPa air and 0.6 MPa methane, and kept for 0.5 h to ensure a dissolution equilibrium with 1,000 RPM min^{-1} magnetic stirring. Subsequently, the reactor was irradiated by 400W Hg-Xe lamp for 2 h. During the reaction, the temperature of the liquid was maintained at 20°C $\pm$ 3°C by an attached cooling system (Minichiller 300). It generates circulating cooling water, which maintains the temperature by contact with the outer wall of the photoreactor. After reaction, the reactor was cooled to 5°C for another 0.5 h without stirring. Then, the gas and liquid products were collected and analyzed.

In the photothermocatalytic process, the photoreactor was equipped with a sand filter to isolate the CsPW-TiO_2 photocatalyst and Ru/Al_2O_3 (Figure S25), in which all

the conditions were the same with the typical process described above except that 1 g commercial 5% Ru/Al_2O_3 was placed in a small glass container on the bottom of reactor. Consequently, CsPW-TiO_2 and Ru/Al_2O_3 can be separated. After irradiation, the 5% Ru/Al_2O_3 was immediately released out from the small glass container by vigorous stirring (1,800 RPM min^{-1}) to oxidize the liquid oxygenates into formic acid at 20°C. Then, the gas and liquid products were collected and analyzed.

The AQY was measured over the CsPW-TiO_2 photocatalyst under 360 nm irradiation with the Hg-Xe lamp equipped with band-pass filter as the light source. The light intensity was measured as 2.7 mW cm^{-2}. Since the formations of CH_3OOH, CH_3OH, and HCHO need 1, 3, and 5 photogenerated charges, respectively, AQY was calculated as follows, where n (CH_3OOH), n (CH_3OH), and n (HCHO) represent the numbers of CH_3OOH, CH_3OH, and HCHO, respectively, and n (photons) represents the number of the irradiated photons during methane conversion.

$$AQY = \frac{\text{Number of used photons}}{\text{Number of incident photons}} = \frac{n(CH_3OOH) + n(CH_3OH) \times 3 + n(HCHO) \times 5}{n(\text{photons})}$$

The gas products were directly injected into GC (PerkinElmer Clarus 580 GC) through a Swagelok tube and analyzed by PoraBOND Q and ShinCarbon ST 100/120 columns with Ar as the carrier gas, accompanied by a flame ionization detector and a thermal conductivity detector.

The liquid products (formic acid, methanol, methyl hydroperoxide) were quantified by ^1H NMR (BRUKER, Avance HD 300 MHz). Typically, 0.5 mL liquid product was mixed with 0.1 mL D_2O containing 0.05 μL dimethyl sulfoxide (DMSO; Sigma-Aldrich, >99.9%) as internal standard. An ^1H NMR spectrum of the liquid product obtained from photocatalytic aerobic methane oxidation over CsPW-TiO_2 is displayed in Figure S27. The formaldehyde was quantified by colorimetric method as reported previously.[28] The concentration of formaldehyde was determined by the standard curve (Figure S28).

Characterization

The X-ray powder diffraction patterns were measured in the 5°–80° (2θ) range using Cu K_α radiation (λ = 0.1538 nm) on a Bruker AXS D8 instrument. A PerkinElmer Lambda 650S UV-visible spectrometer with an integrating sphere covered with $BaSO_4$ as a reference was used for diffuse reflectance UV-visible spectra measurements.

TEM analysis was carried out on a JEOL 2100 FEG S/TEM microscope operated at 200 kV and equipped with a spherical aberration probe corrector. Before analysis, the samples were dispersed in ethanol and deposited on a holey carbon-coated TEM grid. In STEM, the images were recorded using an HAADF detector with inner and outer diameters of about 73 and 194 mrad. EDS analyses allowing the elemental mapping were performed in the S/TEM using a JEOL Silicon Drift Detector (DrySD60GV, sensor size 60 mm) with a solid angle of approximately 0.6 srad.

The PL spectroscopy measurements were performed on a LabRam HR (Horiba Scientific). For excitation, 325 nm radiation from a diode-pumped solid-state 1 mW laser was used. The spectrophotometer has an entrance slit of 100 mm and is equipped with a 300 lines per mm grating that permits achieving a spectral resolution of 3.8 cm per pixel. The luminescence light was detected with a CCD camera operating at −135°C.

The analysis of paramagnetic species has been performed by continuous-wave (CW) EPR. These experiments were performed on a Bruker ELEXSYS E500 spectrometer operating in X-band (9.5 GHz). The following conditions were used for the *in situ* measurements: a microwave power of 2 mW, modulation amplitude of 1 G with a conversion time of 40 ms, and 50 scans. The EPR spectra were recorded at 120 K to avoid electron-hole recombination. The spin-trapping experiments were performed with [DMPO] = 80 mM, microwave power of 10 mW, modulation amplitude of 0.2 G, a conversion time of 5 ms, and 100 scans. An EPR quick pressure tube is used to work under a controlled atmosphere. The spectra were simulated using WinSim software.

SUPPLEMENTAL INFORMATION

Supplemental information can be found online at https://doi.org/10.1016/j.xcrp.2023.101277.

ACKNOWLEDGMENTS

This research is being performed within the ANR SolarMethaChem project (ANR-20-SODR-0002). The authors gratefully acknowledge the support of the French National Research Agency (ANR). D.H. thanks the China Scholarship Council for a PhD stipend. The Chevreul Institute (FR 2638), Ministère de l'Enseignement Supérieur, de la Recherche et de l'Innovation, Région Hauts de France, and FEDER are acknowledged for supporting and partially funding this work.

AUTHOR CONTRIBUTIONS

D.H., V.V.O., and A.Y.K. conceived the idea of the work. D.H. designed the experiments, analyzed the data, and wrote the manuscript. A.A. performed microscopy measurements and analysis. K.B.T. conducted *in situ* EPR measurements and analysis. All authors reviewed the manuscript and agreed on its content.

DECLARATION OF INTERESTS

The authors declare no competitive interests.

INCLUSION AND DIVERSITY

We support inclusive, diverse, and equitable conduct of research.

Received: September 30, 2022
Revised: December 11, 2022
Accepted: January 12, 2023
Published: January 30, 2023

REFERENCES

1. Ma, J., Tan, X., Zhang, Q., Wang, Y., Zhang, J., and Wang, L. (2021). Exploring the size effect of Pt nanoparticles on the photocatalytic nonoxidative coupling of methane. ACS Catal. *11*, 3352–3360. https://doi.org/10.1021/acscatal.0c04943.

2. Jiang, W., Low, J., Mao, K., Duan, D., Chen, S., Liu, W., Pao, C.W., Ma, J., Sang, S., Shu, C., et al. (2021). Pd-modified ZnO–Au enabling alkoxy intermediates formation and dehydrogenation for photocatalytic conversion of methane to ethylene. J. Am. Chem. Soc. *143*, 269–278. https://doi.org/10.1021/jacs.0c10369.

3. Li, Q., Ouyang, Y., Li, H., Wang, L., and Zeng, J. (2022). Photocatalytic conversion of methane: recent advancements and prospects. Angew. Chem. Int. Ed. Engl. *61*, e202108069. https://doi.org/10.1002/anie.202108069.

4. Yang, J., Xiao, W., Chi, X., Lu, X., Hu, S., Wu, Z., Tang, W., Ren, Z., Wang, S., Yu, X., et al. (2020). Solar-driven efficient methane catalytic oxidation over epitaxial ZnO/$La_{0.8}Sr_{0.2}CoO_3$ heterojunctions. Appl. Catal. B Environ. *265*, 118469. https://doi.org/10.1016/j.apcatb.2019.118469.

5. Li, X., Xie, J., Rao, H., Wang, C., and Tang, J. (2020). Platinum- and CuO_x-decorated TiO_2 photocatalyst for oxidative coupling of methane to C_2 hydrocarbons in a flow reactor. Angew. Chem. Int. Ed. Engl. *59*, 19702–19707. https://doi.org/10.1002/anie.202007557.

6. Song, H., Meng, X., Dao, T.D., Zhou, W., Liu, H., Shi, L., Zhang, H., Nagao, T., Kako, T., and Ye, J. (2018). Light-enhanced carbon dioxide activation and conversion by effective plasmonic coupling effect of Pt and Au nanoparticles. ACS Appl. Mater. Interfaces *10*, 408–416. https://doi.org/10.1021/acsami.7b13043.

7. Song, H., Meng, X., Wang, Z.j., Liu, H., and Ye, J. (2019). Solar-energy-Mediated methane conversion. Joule *3*, 1606–1636. https://doi.org/10.1016/j.joule.2019.06.023.

8. Meng, X., Cui, X., Rajan, N.P., Yu, L., Deng, D., and Bao, X. (2019). Direct methane conversion under mild condition by thermo-electro-or photocatalysis. Chem *5*, 2296–2325. https://doi.org/10.1016/j.chempr.2019.05.008.

9. Meng, L., Chen, Z., Ma, Z., He, S., Hou, Y., Li, H.H., Yuan, R., Huang, X.H., Wang, X., Wang, X., et al. (2018). Gold plasmon-induced photocatalytic dehydrogenative coupling of methane to ethane on polar oxide surfaces. Energy Environ. Sci. *11*, 294–298. https://doi.org/10.1039/c7ee02951a.

10. Tang, P., Zhu, Q., Wu, Z., and Ma, D. (2014). Methane activation: the past and future. Energy Environ. Sci. *7*, 2580–2591. https://doi.org/10.1039/c4ee00604f.

11. Nisbet, E.G., Fisher, R.E., Lowry, D., France, J.L., Allen, G., Bakkaloglu, S., Broderick, T.J., Cain, M., Coleman, M., Fernandez, J., et al. (2020). Methane mitigation: methods to reduce emissions, on the path to the paris agreement. Rev. Geophys. *58*, 1–51. https://doi.org/10.1029/2019RG000675.

12. Schuur, E.A.G., McGuire, A.D., Schädel, C., Grosse, G., Harden, J.W., Hayes, D.J., Hugelius, G., Koven, C.D., Kuhry, P., Lawrence, D.M., et al. (2015). Climate change and the permafrost carbon feedback. Nature *520*, 171–179. https://doi.org/10.1038/nature14338.

13. Hu, D., Ordomsky, V.V., and Khodakov, A.Y. (2021). Major routes in the photocatalytic methane conversion into chemicals and fuels under mild conditions. Appl. Catal. B Environ. *286*, 119913. https://doi.org/10.1016/j.apcatb.2021.119913.

14. Lang, J., Ma, Y., Wu, X., Jiang, Y., and Hu, Y.H. (2020). Highly efficient light-driven methane coupling under ambient conditions based on an integrated design of a photocatalytic system. Green Chem. *22*, 4669–4675. https://doi.org/10.1039/d0gc01608j.

15. Chernyak, S.A., Corda, M., Dath, J.-P., Ordomsky, V.V., and Khodakov, A.Y. (2022). Light olefin synthesis from a diversity of renewable and fossil feedstocks: state-of the-art and outlook. Chem. Soc. Rev. *51*, 7994–8044. https://doi.org/10.1039/D1CS01036K.

16. Ordomsky, V.V., and Khodakov, A.Y. (2017). Syngas to chemicals: the incorporation of aldehydes into fischer–tropsch synthesis. ChemCatChem *9*, 1040–1046. https://doi.org/10.1002/cctc.201601508.

17. Luk, H.T., Mondelli, C., Ferré, D.C., Stewart, J.A., and Pérez-Ramírez, J. (2017). Status and prospects in higher alcohols synthesis from syngas. Chem. Soc. Rev. *46*, 1358–1426. https://doi.org/10.1039/C6CS00324A.

18. Chinchen, G.C., Denny, P.J., Jennings, J.R., Spencer, M.S., and Waugh, K.C. (1988). Synthesis of methanol. Appl. Catal. *36*, 1–65. https://doi.org/10.1016/S0166-9834(00)80103-7.

19. Johnson, G.E., Decker, W.A., Forney, A.J., and Field, J.H. (1968). Hydrogen cyanide produced from coal and ammonia. Ind. Eng. Chem. Proc. Des. Dev. *7*, 137–143. https://doi.org/10.1021/i260025a027.

20. Yu, X., De Waele, V., Löfberg, A., Ordomsky, V., and Khodakov, A.Y. (2019). Selective photocatalytic conversion of methane into carbon monoxide over zinc-heteropolyacid-titania nanocomposites. Nat. Commun. *10*, 700. https://doi.org/10.1038/s41467-019-08525-2.

21. Yuliati, L., and Yoshida, H. (2008). Photocatalytic conversion of methane. Chem. Soc. Rev. *37*, 1592–1602. https://doi.org/10.1039/b710575b.

22. Chen, G., Waterhouse, G.I.N., Shi, R., Zhao, J., Li, Z., Wu, L.Z., Tung, C.H., and Zhang, T. (2019). From solar energy to fuels: recent advances in light-driven C_1 chemistry. Angew. Chem. Int. Ed. Engl. *58*, 17528–17551. https://doi.org/10.1002/anie.201814313.

23. Chen, X., Li, Y., Pan, X., Cortie, D., Huang, X., and Yi, Z. (2016). Photocatalytic oxidation of methane over silver decorated zinc oxide nanocatalysts. Nat. Commun. *7*, 12273. https://doi.org/10.1038/ncomms12273.

24. Ward, M.D., Brazdil, J.F., Mehandru, S.P., and Anderson, A.B. (1987). Methane photoactivation on copper molybdate. An experimental and theoretical study. J. Phys. Chem. *91*, 6515–6521. https://doi.org/10.1021/j100310a019.

25. Zhu, W., Shen, M., Fan, G., Yang, A., Meyer, J.R., Ou, Y., Yin, B., Fortner, J., Foston, M., Li, Z., et al. (2018). Facet-dependent enhancement in the activity of bismuth vanadate microcrystals for the photocatalytic conversion of methane to methanol. ACS Appl. Nano Mater. *1*, 6683–6691. https://doi.org/10.1021/acsanm.8b01490.

26. Zhou, Y., Zhang, L., and Wang, W. (2019). Direct functionalization of methane into ethanol over copper modified polymeric carbon nitride via photocatalysis. Nat. Commun. *10*, 506. https://doi.org/10.1038/s41467-019-08454-0.

27. Jiang, Y., Fan, Y., Li, S., and Tang, Z. (2023). Photocatalytic methane conversion: insight into the mechanism of $C(sp^3)$-H bond activation. CCS Chem. *5*, 30–54. https://doi.org/10.31635/ccschem.022.202201991.

28. Song, H., Meng, X., Wang, S., Zhou, W., Wang, X., Kako, T., and Ye, J. (2019). Direct and selective photocatalytic oxidation of CH_4 to oxygenates with O_2 on cocatalysts/ZnO at room temperature in water. J. Am. Chem. Soc. *141*, 20507–20515. https://doi.org/10.1021/jacs.9b11440.

29. Zhou, W., Qiu, X., Jiang, Y., Fan, Y., Wei, S., Han, D., Niu, L., and Tang, Z. (2020). Highly selective aerobic oxidation of methane to methanol over gold decorated zinc oxide: via photocatalysis. J. Mater. Chem. A *8*, 13277–13284. https://doi.org/10.1039/d0ta02793f.

30. Song, H., Meng, X., Wang, S., Zhou, W., Song, S., Kako, T., and Ye, J. (2020). Selective photo-oxidation of methane to methanol with oxygen over dual-cocatalyst-modified titanium dioxide. ACS Catal. *10*, 14318–14326. https://doi.org/10.1021/acscatal.0c04329.

31. Xie, J., Jin, R., Li, A., Bi, Y., Ruan, Q., Deng, Y., Zhang, Y., Yao, S., Sankar, G., Ma, D., et al. (2018). Highly selective oxidation of methane to methanol at ambient conditions by titanium dioxide-supported iron species. Nat. Catal. *1*, 889–896. https://doi.org/10.1038/s41929-018-0170-x.

32. Ohkubo, K., and Hirose, K. (2018). Light-driven C−H oxygenation of methane into methanol and formic acid by molecular oxygen using a perfluorinated solvent. Angew. Chem. Int. Ed. Engl. *57*, 2126–2129. https://doi.org/10.1002/anie.201710945.

33. Wei, S., Zhu, X., Zhang, P., Fan, Y., Sun, Z., Zhao, X., Han, D., and Niu, L. (2021). Aerobic oxidation of methane to formaldehyde mediated by crystal-O over gold modified tungsten trioxide via photocatalysis. Appl. Catal. B Environ. *283*, 119661. https://doi.org/10.1016/j.apcatb.2020.119661.

34. Sun, Z., Wang, C., and Hu, Y.H. (2021). Highly selective photocatalytic conversion of methane to liquid oxygenates over silicomolybdic-Acid/TiO_2 under mild conditions. J. Mater. Chem. A *9*, 1713–1719. https://doi.org/10.1039/d0ta09226f.

35. Rojas-Andrade, M.D., and Chen, S. (2018). Structural engineering of nanoparticle catalysts for electrochemical oxidation of formic acid. In Encyclopedia of Interfacial Chemistry (Elsevier), pp. 863–880. https://doi.org/10.1016/B978-0-12-409547-2.13319-0.

36. Kawanami, H., Himeda, Y., and Laurenczy, G. (2017). Formic acid as a hydrogen carrier for fuel cells toward a sustainable energy system. Adv. Inorg. Chem. *70*, 395–427. https://doi.org/10.1016/bs.adioch.2017.04.002.

37. Ogura, K., and Kataoka, M. (1988). Photochemical conversion of methane. J. Mol. Catal. *43*, 371–379. https://doi.org/10.1016/0304-5102(88)85148-4.

38. Murcia-López, S., Villa, K., Andreu, T., and Morante, J.R. (2014). Partial oxidation of methane to methanol using bismuth-based photocatalysts. ACS Catal. *4*, 3013–3019. https://doi.org/10.1021/cs500821r.

39. Jiang, Y., Zhao, W., Li, S., Wang, S., Fan, Y., Wang, F., Qiu, X., Zhu, Y., Zhang, Y., Long, C., et al. (2022). Elevating photooxidation of methane to formaldehyde via TiO_2 crystal phase engineering. J. Am. Chem. Soc. *144*, 15977–15987. https://doi.org/10.1021/jacs.2c04884.

40. Cotta, R.F., da Silva Rocha, K.A., Kozhevnikova, E.F., Kozhevnikov, I.V., and Gusevskaya, E.V. (2017). Heteropoly acid catalysts in upgrading of biorenewables: cycloaddition of aldehydes to monoterpenes in green solvents. Appl. Catal. B Environ. *217*, 92–99. https://doi.org/10.1016/j.apcatb.2017.05.055.

41. Yu, X., Zholobenko, V.L., Moldovan, S., Hu, D., Wu, D., Ordomsky, V.V., and Khodakov, A.Y. (2020). Stoichiometric methane conversion to ethane using photochemical looping at ambient temperature. Nat. Energy *5*, 511–519. https://doi.org/10.1038/s41560-020-0616-7.

42. Matachowski, L., Zimowska, M., Mucha, D., and Machej, T. (2012). Ecofriendly production of ethylene by dehydration of ethanol over $Ag_3PW_{12}O_{40}$ salt in nitrogen and air atmospheres. Appl. Catal. B Environ. *123–124*, 448–456. https://doi.org/10.1016/j.apcatb.2012.05.003.

43. Meng, P., Heng, H., Sun, Y., Huang, J., Yang, J., and Liu, X. (2018). Positive effects of phosphotungstic acid on the in-situ solid-state polymerization and visible light

photocatalytic activity of polyimide-based photocatalyst. Appl. Catal. B Environ. *226*, 487–498. https://doi.org/10.1016/j.apcatb.2018.01.004.

44. Wang, H., Zhang, L., Chen, Z., Hu, J., Li, S., Wang, Z., Liu, J., and Wang, X. (2014). Semiconductor heterojunction photocatalysts: design, construction, and photocatalytic performances. Chem. Soc. Rev. *43*, 5234–5244. https://doi.org/10.1039/c4cs00126e.

45. Chen, X., and Burda, C. (2008). The electronic origin of the visible-light absorption properties of C-N- and S-doped TiO_2 nanomaterials. J. Am. Chem. Soc. *130*, 5018–5019. https://doi.org/10.1021/ja711023z.

46. Wang, K., Li, Y., Zhang, G., Li, J., and Wu, X. (2019). 0D Bi nanodots/2D Bi_3NbO_7 nanosheets heterojunctions for efficient visible light photocatalytic degradation of antibiotics: enhanced molecular oxygen activation and mechanism insight. Appl. Catal. B Environ. *240*, 39–49. https://doi.org/10.1016/j.apcatb.2018.08.063.

47. Ai, S., Wang, Q., Li, H., and Jin, L. (2005). Study on production of free hydroxyl radical and its reaction with salicylic acid at lead dioxide electrode. J. Electroanal. Chem. *578*, 223–229. https://doi.org/10.1016/j.jelechem.2005.01.002.

48. Luo, L., Gong, Z., Xu, Y., Ma, J., Liu, H., Xing, J., and Tang, J. (2022). Binary Au–Cu reaction sites decorated ZnO for selective methane oxidation to C_1 oxygenates with nearly 100% selectivity at room temperature. J. Am. Chem. Soc. *144*, 740–750. https://doi.org/10.1021/jacs.1c09141.

49. Hoffmann, M.R., Martin, S.T., Choi, W., and Bahnemann, D.W. (1995). Environmental applications of semiconductor photocatalysis. Chem. Rev. *95*, 69–96. https://doi.org/10.1021/cr00033a004.

50. Fan, Y., Zhou, W., Qiu, X., Li, H., Jiang, Y., Sun, Z., Han, D., Niu, L., and Tang, Z. (2021). Selective photocatalytic oxidation of methane by quantum-sized bismuth vanadate. Nat. Sustain. *4*, 509–515. https://doi.org/10.1038/s41893-021-00682-x.

51. Zhang, X., Li, Z., Zeng, B., Li, C., and Han, H. (2022). EPR study of charge separation associated states and reversibility of surface bound superoxide radicals in $SrTiO_3$ photocatalyst. J. Energy Chem. *70*, 388–393. https://doi.org/10.1016/j.jechem.2022.02.038.

52. Anglada, J.M., Crehuet, R., Martins-Costa, M., Francisco, J.S., and Ruiz-López, M. (2017). The atmospheric oxidation of CH_3OOH by the OH radical: the effect of water vapor. Phys. Chem. Chem. Phys. *19*, 12331–12342. https://doi.org/10.1039/C7CP01976A.

53. Schneider, J., and Bahnemann, D.W. (2013). Undesired role of sacrificial reagents in photocatalysis. J. Phys. Chem. Lett. *4*, 3479–3483. https://doi.org/10.1021/jz4018199.

54. Qin, X., Chen, X., Chen, M., Zhang, J., He, H., and Zhang, C. (2021). Highly efficient Ru/CeO_2 catalysts for formaldehyde oxidation at low temperature and the mechanistic study. Catal. Sci. Technol. *11*, 1914–1921. https://doi.org/10.1039/d0cy01894e.

55. Gao, H., Yan, T., Zhang, C., and He, H. (2008). Theoretical and experimental analysis on vibrational spectra of formate species adsorbed on $Cu\text{-}Al_2O_3$ catalyst. J. Mol. Struct.: THEOCHEM *857*, 38–43. https://doi.org/10.1016/j.theochem.2008.02.004.

56. Danilevich, E.v., Popova, G.Y., Zolotarskii, I.A., Ermakova, A., and Andrushkevich, T.v. (2010). Kinetics of formaldehyde oxidation on a vanadia-titania catalyst. Catal. Ind. *2*, 320–328. https://doi.org/10.1134/S2070050410040057.